Journal Pre-proof

Tuning amino acid dehydrogenases with featured sequences for L-phosphinothricin synthesis by reductive amination

Feng Cheng (Conceptualization) (Investigation) (Writing - original draft), Heng Li (Data curation) (Writing - original draft) (Methodology), Kai Zhang (Visualization) (Investigation), Qing-Hua Li (Data curation) (Investigation), Dong Xie (Visualization), Ya-Ping Xue<ce:contributor-role>Writing- Review and editing) (Project administration), Yu-Guo Zheng (Supervision)

PII: S0168-1656(20)30050-X

DOI: https://doi.org/10.1016/j.jbiotec.2020.03.001

Reference: BIOTEC 8611

To appear in: *Journal of Biotechnology*

Received Date: 19 December 2019

Revised Date: 16 February 2020

Accepted Date: 1 March 2020

Please cite this article as: { doi: https://doi.org/

Tuning amino acid dehydrogenases with featured sequences for L-phosphinothricin synthesis by reductive amination

Feng Cheng [1,2], Heng Li [1,2], Kai Zhang [1,2], Qing-Hua Li [1,2], Dong Xie [1,2], Ya-Ping Xue [1,2,*] and Yu-Guo Zheng [1,2]

1. Key Laboratory of Bioorganic Synthesis of Zhejiang Province, College of Biotechnology and Bioengineering, Zhejiang University of Technology, Hangzhou, 310014, P. R. China.
2. The National and Local Joint Engineering Research Center for Biomanufacturing of Chiral Chemicals, Zhejiang University of Technology, Hangzhou, 310014, P. R. China.

Corresponding author:

Prof. Ya-Ping Xue

College of Biotechnology and Bioengineering,

Zhejiang University of Technology,

Hangzhou 310014, P. R. China

Tel: +86-571-88320391

E-mail: xyp@zjut.edu.cn

Graphic abstract

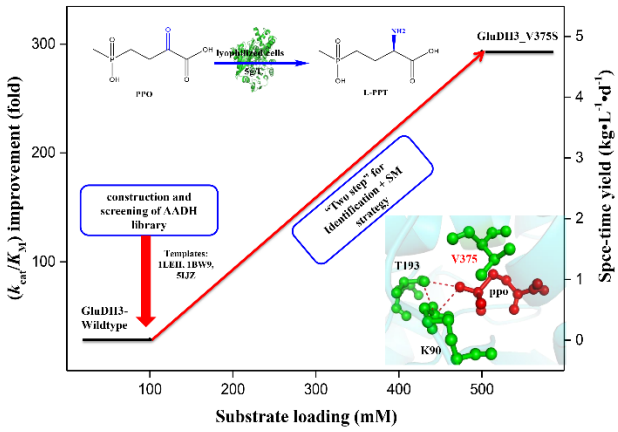

Highlights

- A new *in silico* method was developed for discovery of glutamate dehydrogenase.
- An *in silic*o and experiment combined strategy was developed for a prediction of glufosinate dehydrogenase with desired asymmetric reductive amination activity.
- Forty newly engineered glutamate dehydrogenases with specific features showed the reductive amination activity toward 2-oxo-4-[(hydroxy)(methyl) phosphinoyl]butyric acid.
- A high space-time yield of L-phosphinothricin up to 4.752 kg $L^{-1}\cdot d^{-1}$ was reached by using *E. coli* cell co-expressing GluDH3_V375S and *Es*GDH as biocatalyst.

Abstract

Biosynthesizing unnatural chiral amino acids is challenging due to the limited reductive amination activity of amino acid dehydrogenase (AADH). Here, for the asymmetric synthesis of L-phosphinothricin from 2-oxo-4-[(hydroxy)(methyl)phosphinoyl]butyric acid (PPO), a glutamate dehydrogenase gene (named GluDH3) from *Pseudomonas monteilii* was selected, cloned and expressed in *Escherichia coli* (*E. coli*). To boost its activity, a "two-step"-based computational approach was developed and applied to select the potential beneficial amino acid positions on GluDH3. L-phosphinothricin was synthesized by GluDH-catalyzed asymmetric amination using the D-glucose dehydrogenase from *Exiguobacterium sibiricum* (*Es*GDH) for NADPH regeneration.

Using lyophilized *E. coli* cells that co-expressed GluDH3_V375S and *Es*GDH, up to 89.04 g L^{-1} PPO loading was completely converted to L-phosphinothricin within 30 min at 35 °C with a space-time yield of up to 4.752 kg·L^{-1}·d^{-1}. The beneficial substitution V375S with increased polar interactions between K90, T193, and substrate PPO exhibited 168.2-fold improved catalytic efficiency (k_{cat}/K_M) and 344.8-fold enhanced specific activity. After the introduction of serine residues into other GluDHs at specific positions, forty engineered GluDHs exhibited the catalytic functions of "glufosinate dehydrogenase" towards PPO.

Keywords: Amino acid dehydrogenase; Semi-rational engineering; Asymmetric synthesis; L-phosphinothricin

1 Introduction

The asymmetric synthesis of unnatural amino acids using amino acid dehydrogenases (AADHs) as catalysts has attracted significant interest because of its high atom economy and brief reaction steps (Sharma et al., 2018; Xue et al., 2018). This route is thermodynamically favorable because of its high equilibrium constant (K_{eq}) of 10^{14}-10^{18} (Zhu and Hua, 2009). Although the nicotinamide cofactor NAD(P)H used in the reaction is expensive for industrial applications, an efficient regeneration system involving D-glucose dehydrogenase (GDH)/glucose enables reuse cofactors (Ricca et al., 2011; Singh et al., 2012; Srivastava et al., 2015; Uppada et al., 2014). The AADH superfamily contains different groups according to their natural substrates (Brunhuber and Blanchard, 1994; Bommarius et al., 2015; Hummel et al., 2012) such as glutamate dehydrogenases (GluDHs), phenylalanine dehydrogenases (PheDHs) and leucine dehydrogenases (LeuDHs), which have been widely applied. Homology-based modeling studies have shown that they share similar structures containing two domains, which consist of a substrate-binding domain and a cofactor-binding domain, and the substrate lies deep within the cleft between the two domains (Baker et al., 1997; Tomita et al., 2017). More importantly, the basis of the differential substrate specificity between these enzymes involves point mutations in the substrate-binding pocket and subtle changes in the shape of the pocket caused by differences in the quaternary structure (Seah et al., 1995). Thus, introducing a small number of amino acid substitutions could extend the enzyme substrate scope or enhance the enzyme activity (Busca et al., 2004; Geng et al., 2017; Xu et al., 2017; Prakash et al., 2018).

To date, with the development of protein engineering, the substrate scope of AADHs has been expanded, to some extent (Sharma et al., 2017). Engineered AADH variants have been successfully applied to the production of non-natural products through the substitution of key residues in the active sites of AADHs (Li and Liao, 2014; Zhu et al., 2016). However, the synthesis of non-natural amino acids containing heteroatoms was still a bottleneck for AADHs, such as PheDH toward 4-CF_3-phenyl pyruvate and 2-thienyl pyruvate (Busca et al., 2004; Paradisi et al., 2007).

L-phosphinothricin (2-amino-4-[(hydroxyl)(methy)phosphonoyl]butanoic acid, L-PPT, also known as L-glufosinate) is an unnatural chiral amino acid containing phosphorus atoms, and it is used as a non-selective, foliar-applied herbicide (Tan et al., 2006; Hoerlein, 1994) due to its inhibiting effect on glutamine synthetase, which is involved in the general nitrogen metabolism of plants (Brunharo et al., 2019). During recent decades, considerable efforts have been dedicated to developing efficient and sustainable enzymatic methods for synthesizing L-PPT, as exemplified by the reactions catalyzed by transaminases (Jia et al., 2019; Jin et al., 2019; Cheng et al., 2020), deacetylase (Bartsch et al., 2001), amidase (Kang et al., 2019a), and nitrilase (Albizati et al., 2017). Undeniably, these enzymes exhibited appropriate stereoselectivity and higher productivity during L-PPT production. However, transaminase-catalyzed reactions are reversible, and approximately 20% PPO still remains in the reaction mixture (Jia et al., 2019); thus, a difficult L-PPT and PPO separation process is required, which would not benefit the industrialization of L-PPT production. Deacetylase and amidase-catalyzed reactions can only achieve a theoretical maximum yield of 50% (Kang et al., 2019a). Using nitrilase involves methods that require a hazardous, nitrile-containing substrate, which does not meet the criteria for "green chemistry" (Bartsch et al., 2001). Although the AADH-catalyzed reactions have some advantages such as a high stereoselectivity, theoretical maximum yield (100%) and equilibrium constant (Khorsand et al., 2017), natural AADH rarely catalyzed the reductive amination of prochiral PPO due to the challenge of tolerating the phosphoryl group in PPO for asymmetric reductive amination.

In this study, a glutamate dehydrogenase (GluDH3) was mined, and its activity was boosted by semi-rational engineering. GluDH3_WT and GluDH3_V375S were characterized and the role of the beneficial substitutions was investigated. A strategy was developed to engineer forty glutamate dehydrogenases into "glufosinate dehydrogenase". The asymmetric reductive amination

of high-concentration PPO was tested by employing whole cells of recombinant *E. coli* harboring GfDH and GDH.

2 Materials and Methods

2.1 Microorganisms and Materials

E. coli strain BL21(DE3) was purchased for use as a host for gene expression and protein production from TransGen Biotech (Beijing, China). Phanta Max Super-Fidelity DNA Polymerase for mutagenesis was purchased from Vazyme (Nanjing, China). SDS-PAGE, Bis-Tris buffer and a BCA protein assay kit were purchased from GenScript (Nanjing, China). Plasmid Miniprep kits and DNA gel extraction kits were purchased from Axygen Scientific, Inc. (Hangzhou, China). PPO was obtained from Yong Nong, Inc. (Hangzhou, China). Racemic D,L-PPT was purchased from J&K Scientific (Beijing, China). All the other chemicals and regents used in this study were chemically pure and were purchased commercially.

2.2 Analytical methods

The PPO concentration was determined by high performance liquid chromatography (HPLC) on a C18 column (Unitary C 18, 5 μm, 100 A, 4.6 mm × 250 mm) at a flow rate of 1.0 mL/min and detected at a wavelength of 232 nm. Each sample (10 μL) was eluted with 50 mM ammonium dihydrogen phosphate (pH 3.8) buffer containing 0.1% tetrabutyl ammonium bromide and 12% acetonitrile as the mobile phase. The column temperature was maintained at 40 °C. The retention time of PPO was 9.4 min.

The concentration and excess (*e.e.*) of optical L-PPT were determined at fluorescence wavelengths of λ_{ex}= 340 nm and λ_{em}= 450 nm after 5 minutes of derivatization using *o*-phthalaldehyde (OPA) and N-acetyl-L-cysteine (NAC) at 30 °C in the same HPLC instrument and column. The column temperature and the flow rate of the mobile phase were also the same as those above. The only difference is that the mobile phase was also pH 3.7, with 50 mM ammonium acetate and methanol (9:1 v/v). The retention time of L-PPT was 13.6 min.

2.3 Homology modeling, docking and MD simulations

Protein structure modeling was implemented with MODELLER ver. 9.20 using the *Cg*GluDH (a GluDH from *Corynebacterium glutamicum*) structure (PDB ID: 5IJZ, 2.3 Å) as the template. The

structure with the highest score was repaired with FoldX and the substrate structure was prepared with ChemOffice Pro software before the docking and MD simulations. All the docking calculations were performed in AutoDock 4.0 and six residues (K90, A164, T193, V375, S378, and G379) in the protein binding pockets were set as flexible residues. MD simulations were performed using GROMACS 5.0. The topological structure of the ligand was generated with the PRODRG server online, and the errors in the atoms were amended artificially. An Amber03 force field and a temperature of 300 K were adopted for the protein, and the TIP3P water model was used to solvate each system. The simulation time was set to 30 ns. The stereoview images of GluDH in holo form were constructed using PyMOL software.

2.4 Mutant library construction and screening

The site-saturation mutagenesis of GluDH was performed using a QuikChange Mutagenesis Kit with a Phanta Max Super-Fidelity DNA Polymerase (Vazyme, Nanjing, China). All the primers (**Table S1**) were designed with the Prime X online service. The PCR conditions for the fragment were as follows: 95 ℃ for 5 min, (90 ℃ 30 s, 60 ℃-70 ℃ for 30 s, 72 ℃ for 7 min) ×30 cycles, and 72 ℃ for 10 min. The PCR products were analyzed on an agarose gel following electrophoresis. Following digestion at 37 ℃ for 15 min (1 μL of DpnI and 5 μL of cut-smart buffer with 50 μL of PCR products), the PCR products were directly transformed into *E. coli* BL21 (DE3) competent cells by chemical method.

Single colonies were picked and inoculated into 1.0 mL of LB medium (50 μg/mL ampicillin) in each well of a 96-well plate after obtaining the transformants, and the cultures were incubated for 10 h at 37 ℃ and 180 rpm. Subsequently, 200 μL of seeding culture from each well was transferred to another 96-well plate containing 800 μL of LB medium (containing 62.5 μg/mL ampicillin and 0.1 mM IPTG) and cultivated at 18 ℃ for 18 h (180 rpm). The cultures were centrifuged at 4000 rpm for 10 min and the cells were re-suspended in 250 μL of 0.1 M phosphate buffer (pH 7.2). The reaction (500 μL) contained phosphate, 5.0 mM PPO, 10.0 mM ammonium and 6.0 mM glucose and was performed at 35 ℃ in a Thermomixer Compact (Eppendorf, Germany) for 2.0 h. Centrifugation was used to stop the reactions. OPA (5 mM) and NAC (2.5 mM) were added to the supernatants, which were allowed to stand at 30 ℃ for 5 min in black 96-well plates before being

measured at λ_{ex}= 340 nm and λ_{em}= 450 nm wavelengths to detect their activity. The beneficial variants were sequenced and stored in 30% glycerin solution at -80 °C.

2.5 Expression and purification of enzymes

Recombinant *E. coli* cells were inoculated into 50 mL of LB medium containing 50 μg/mL ampicillin and grown at 37 °C for 8 h. Then, 2 mL of cell culture was transferred into 100 mL of fresh LB medium containing 50 μg/mL ampicillin and incubated for another 2 h. Enzyme expression was induced by adding IPTG (0.1 mM final concentration) when the OD_{600} ranged from 0.4-0.6. After 16 h of incubation at 18 °C, the cells were harvested by centrifugation at 8,000 rpm and 4 °C for 10 min. The precipitate was resuspended in buffer A (50 mM phosphate buffer pH 7.0 containing 500 mM NaCl). The cells were disrupted by ultrasonication for 10 min (1 sec on, 1 sec off), and the suspension was centrifuged at 12,000 rpm for 10 min to yield a clear lysate. The N-terminal His_6-tagged protein was purified using IMAC on a Nickel-NTA column (Bio-Rad, CA) by eluting with buffer B (buffer A containing 500 mM imidazole). The purity and molecular weight of the collected protein were analyzed by SDS-PAGE, and the concentration was determined with a BCA protein assay kit.

2.6 Characterizations of the enzyme

Standard enzyme activity assay: the enzyme activities of the purified enzymes were measured at 35 °C in 0.1 M phosphate buffer (Na_2HPO_4-NaH_2PO_4, pH 6.5). The final volume was 1 mL, and it contained 20 mM PPO, 50 mM $(NH_4)_2SO_4$, 10 mM NADPH, and enzyme. The entire mixture except the enzyme was pre-incubated for 5 min at the same temperature. After reacting for 5 min with shaking at 600 rpm, the reaction was terminated by adding 10 μL of 6 M HCL, and the reacted solution was centrifuged at 12000 rpm for 1 min. The supernatant was filtered and analyzed by HPLC, as described in the "analytical methods" section. One unit of enzyme activity (U) was defined as the amount of enzyme required to produce 1 μmol L-PPT per minute under standard enzyme activity assay conditions.

To optimize the reaction pH, the enzyme activity was determined at 35 °C using a different buffer containing acetate buffer (pH 5-6), phosphate buffer (pH 6-8), and Tris-HCl buffer (pH 7-9) at the same concentration. To optimize the reaction temperature, the enzyme activity was measured in phosphate buffer (pH = 6.5) at different temperatures (20-70 °C). To investigate the enzyme

thermostability, purified enzymes were subjected to temperatures of 25 °C, 35 °C, and 45 °C for 0-24 h, and then their activity was measured using the enzyme maintained under standard enzyme activity assay conditions. The kinetic parameters were measured with 0.5 mM to 20 mM PPO and 1 mM to 10 mM NADPH, and the ammonium concentration was fixed at 0.1 M. The turnover number (k_{cat}) and Michaelis constant (K_M) were calculated based on the Lineweaver-Burk plot using the following equation. The kinetic constants were measured through non-linear regression based on Michaelis-Menten kinetics with Origin software. Double reciprocal plots of the initial rates were constructed when the concentration of one substrate varied at different fixed concentrations of a second substrate (NADPH), with the third substrate (ammonium) held at saturation.

$$v = \frac{v_{max[A][B]}}{[A][B] + [B]K_m^A + [A]K_{m+}^B K_m^B K_s^A}$$

Where [A] and [B] are the concentrations of NADPH and PPO, respectively. v_{max} is the maximum reaction rate, and K_M^A and K_M^B are the apparent substrate affinities toward NADPH and PPO, respectively. Ks^A represents the dissociation constant between GfDH and NADPH.

2.7 Asymmetric amination of PPO using recombinant *E. coli* cells

The asymmetric amination of PPO for the preparation of *L*-PPT was performed with 0.15 g of lyophilized *E. coli* BL21 cells overexpressing GluDH3 and GDH, 3.0-15.0 mmol PPO, 4.2-18 mmol (1.2 times molar ratio of PPO) glucose, 0.0075 mmol $NADP^+$, and 4.5-22.5 mmol ammonium sulfate dissolved in 30 mL of phosphate buffer (0.1 M, pH 6.5). The reactions were magnetically agitated at 350 rpm and 35 °C and maintained at a pH of 6.5 using 12.0 M ammonium hydroxide in a pH-Stat. Samples were taken from the reaction mixture at different time points, and the product concentration and enantioselectivity were analyzed as mentioned above after centrifugation at 12,000 rpm for 2 min.

2.8 Data analysis

All the data were obtained from triplicate measurements and represented as the means ± standard deviations (SD). A statistical analysis was performed using SAS program version 8.1 (SAS Institute Inc., Cary, NC, USA).

3 Results and discussion

3.1 Selection of biocatalyst (AADH) candidates using an *in silico* approach

To identify a suitable biocatalyst candidate for L-PPT synthesis, ten AADH genes were mined and selected from different AADH families using a "two-step" approach. First, the GluDH (PDB ID: 5IJZ) was used as a probe to search sequences that shared >50% sequence similarity in the NCBI database, because GluDHs are theoretically promising biocatalysts for L-PPT synthesis. The structure of the GluDH natural substrate (α-ketoglutarate) is highly similar to that of the target substrate PPO (**Fig. S1**). α-Ketoglutarate has a carboxyl group and PPO harbors a phosphinoyl group that is bulkier than a carboxyl group but less polar. Second, considering the broad substrate scope of LeuDHs and PheDHs (Xue et al., 2018), a LeuDH (PDB ID: 1LEH) and a PheDH (PDB ID: 1BW9) were also used as templates for gene mining to avoid missing potential AADHs with activity towards PPO. Ten genes were mined and synthesized (**Table 1**, E1 to E10). They were cloned into a pETDuet-1 vector and successfully expressed in *E. coli* BL21 (DE3). Four out of ten exhibited higher activity (121.10-328.77 U/g) than other AADHs towards PPO (< 10 U/g, **Table 1**). As expected, all four enzyme genes belonged to the GluDH group. They shared 58%-61% amino acid sequence similarity with the GluDH probe, but they had low shared sequence identities with the LeuDH probe and the PheDH probe (**Fig. 1**). The reason why GluDHs exhibited higher activity appears that the carboxylic acid in the side chain in GluDH is closer to the polar PPO, while the PheDH and LeuDH are not accommodating polar side chains in their active site. Subsequently, enzyme E3 (GluDH3), which showed the highest activity among the four GluDHs, was selected for further study.

3.2 Identification of beneficial GluDH3 variants using the optimized HT screening method from the GluDH3 library

The homology model of GluDH3 was generated based on an NADPH-specific glutamate dehydrogenase from *Corynebacterium glutamicum* (PDB ID: 5IJZ, 2.3 Å) that shared 58% of its amino acid sequence identity with GluDH3 (Son et al., 2015). Subsequently, FoldX software was used for model refinement (Rojas-Cervellera et al., 2013). The model quality was checked using the Verify-3D online service (https://servicesn.mbi.ucla.edu/Verify3D/). Approximately 97.3% of the residues have average 3D-1D scores > 0.2, which indicated that the model is credible. The resulting

refined model contains a typical cofactor-binding domain in the Rossmann fold and a substrate-binding domain, like that of other AADH crystal structures (**Fig. S2**).

A "two-step"-based *in silico* approach was developed to select the potentially beneficial positions in GluDH3. Step I: The positions should be located in the substrate-binding pocket or active site-decorating loops based on the three-dimensional model and previously reports (Baker et al., 1992; Li and Liao, 2014). Therefore, the K90, K114, D166, T193, R205, V375 and S378 positions were considered as hotspots for mutation. All of these hotspots are around a PPO with a distance shorter than 4 Å, indicating that they may have a great impact on the catalytic performance. Step II: Using the proposed glutamate dehydrogenase substrate-binding model (Son et al., 2015), a catalytic mechanism (Prakash et al., 2018) and sequence alignment (**Fig. S3**) were proposed. K114 is one of the residues that can stabilize the negatively charged a-ketoglutarate through charge-charge interaction. Considering the highly similar structures between PPO and a-ketoglutarate, this residue may be essential for stabilizing PPO. D166 is also a residue of the same importance because of its role in stabilizing the α-imino group of the intermediate (Tomita et al., 2017). Additionally, these two residues were highly conserved in all the GluDHs. Thus, K114 and D166 should be excluded. Finally, the K90, T193, R205, V375, and S378 positions were selected for later GluDH3 mutation.

Before library generation and screening, a derivative reaction-based high-throughput method (Cheng et al., 2018; Kang et al., 2019b) was developed in our lab to detect L-PPT. PPT has a strong fluorescence value at specific wavelengths (λ_{ex}= 340 nm, λ_{em}= 450 nm) after reacting with the derivative reagent, and the value is positively correlated with the PPT concentration (ranging from 0.1 mM to 5 mM). Thus, we set the initial PPO concentration to 5 mM for library screening. However, the previously developed assay did not consider the effects of the ammonia donor $(NH_4)_2SO_4$ on the derivative reagent, which leads to increased background and interferes with the screening process. In addition, the higher ammonium concentration benefits the reductive amination process. Hence, we hope that the ammonia concentration does not interfere with the detection of the lower concentration of L-PPT converted by PPO. The concentrations of *N*-acetyl cysteine (NAC) affecting the derivatization and ammonium were then optimized to minimize the interference by ammonium in the HT screening assay (**Fig. S4a**). Finally, the optimal NAC and ammonium concentrations were set to 2.5 mM and 10 mM, respectively (**Fig. S4b**).

Focused libraries were generated using the above-identified positions of 90, 193, 205, 375 and 378 by site-saturation mutagenesis (SSM, using NNK codon). After the gene library generation, 15 colonies from each library were randomly selected for sequencing. The quality of the gene library met the standards when at least five different codons were observed from the 15 colonies (**Table S2**). Ninety-six clones were screened for each position (including three GluDH3_WTs as the reference) using the optimized HT screening method. In total, 38 variants selected from approximately 2000 variants showed 1-7-fold higher activity (as measured by microplate reader) than the WT (**Fig. 2a**). Combined with the protein expression levels, six variants exhibited improved enzyme activity and similar protein production levels compared to the WT. After sequencing, two beneficial substitutions were identified from these six variants, namely V375G and V375S. Variants GluDH3_V375G and GluDH3_V375S displayed the highest enzyme-specific activity towards 20 mM PPO (GluDH3_V375S: 106.69 U/mg, GluDH3_V375G: 76.05 U/mg, GluDH3_WT: 0.31 U/mg, **Fig. 2b**).

3.3 Characterizations of GluDH3_WT and its variants GluDH3_V375S

The kinetic parameters of GluDH3_WT and its "best" variant GluDH3_V375S were determined using purified enzyme (**Fig. S5**) in phosphate buffer (pH = 6.5, 35 °C) to investigate the contribution of beneficial substitutions to GluDH3 activity (**Table 2**). The variant GluDH3_V375S exhibited great improvements in the catalytic efficiency (k_{cat}/K_M) towards PPO compared with the starting GluDH3 (291.02 $mM^{-1}\cdot s^{-1}$ and 1.73 $mM^{-1}\cdot s^{-1}$ for GluDH3_V375S and GluDH3 respectively). Moreover, the enhanced k_{cat}/K_M is primarily attributed to an increase in the k_{cat} (1290.42 s^{-1} and 33.24 s^{-1} for GluDH3_V375S and GluDH3 respectively). Compared with the effects of the other reported AADH (Yin et al., 2018) (k_{cat} = 12.33 s^{-1}) on the substrate PPO, the k_{cat} value of the variant GluDH3_V375S was 104-fold higher than that of the reported AADHs. The specific activity of GluDH3_V375S was 106.69 U/mg, which is significantly higher than that of our GluDH3_WT (344-fold improvement).

The effects of the temperature and pH on the GluDH3_V375S activity was tested over a range from 20 to 70 °C (temperature) and 5.0 to 9.0 (pH). The highest activity was observed at pH 6.5 (phosphate buffer) and 35 °C (**Fig. S6**). When the pH was lower than 6.0 or higher than 7.5, the

relative activities were lower than 80%. Enzyme activity is preferred at temperatures of 20-45 °C. The optimal temperature of the variant GluDH3_V375S was 35 °C, which is the same as the wild type. When the temperature increased to 55 °C, the variant GluDH3_V375S still showed 70% residual activity. Furthermore, the thermal stability of "best" variant GluDH3_V375S was evaluated at 25, 35, and 45 °C. The half-lives ($t_{1/2}$) were 51.2, 36.9, and 27.1 h at 25, 35, and 45 °C, respectively (**Fig. S6**). These findings suggested that variant GluDH3_V375S displayed good thermal stability.

The substrate scopes of GluDH3_WT and GluDH3_V375S were investigated with regards to various α-keto acids with different structures (**Table 4**). The GluDH3_WT exhibited higher activity towards aliphatic α-keto acids than aromatic α-keto acids. For instance, the activities of GluDH3_WT are 9131 U/g for α-ketoglutarate, 222.7 U/g for 2-oxobutyric acid, and 277.5 U/g for 2-oxopentanoic acid. However, for 2-oxo-2-phenylacetic acid and 3-hydroxy-2-oxo-3-phenylpropanoic acid, the activities are only 1.09 and 3.82 U/g, respectively. Variant GluDH3_V375S exhibited dramatically increased activity when the substrate had another polar group, such as PPO and α-ketoglutarate. For the other substrates, GluDH3_V375S showed similar activity to that of GluDH3_WT.

3.4 Analysis of beneficial substitutions *in silico*

To gain structural insights into beneficial substitutions, a docking analysis and MD simulations were performed on GluDH3_WT and its variant GluDH3_V375S. The significant difference between the WT and GluDH3_V375S with substrate PPO is that a new H-bond network was formed between K90, T193 and PPO. In the holo form of the WT with PPO (**Fig. 3a**), an H-bond (N-H···O) was formed between K90 and the phosphoryl group of PPO. When V375 was replaced by serine, additional H-bonds (O-H···O and N-H···O) were formed between T193, K90 and the carbonyl of the phophoryl group of substrates (**Fig. 3b**).

Furthermore, during the 30 ns MD simulations, we found that an H-bond was formed between T193 and PPO over a 30% timespan (≈ 9.0 ns), and the two newly formed H-bonds (T193···PPO and K90···PPO) were formed over a 26% timespan (≈ 7.8 ns) (**Fig. S7**). No such H-bonds were observed in the 30 ns MD simulations of GluDH3_WT with PPO. Taken together, these findings show that the new H-bond network in variant WT+V375S with PPO is more stable compared to that of the WT. Moreover, variant GluDH3_V375S exhibited lower steric hindrance (low K_M value)

due to the decreased hindrance for the methyl group (**Fig. 3 c-d**). Compared with the model of the WT-PPO complex, the phosphoryl group of the PPO rotates 44^{o} in the GluDH3_V375S-PPO complex (**Fig. S8**) and the hydroxyl group of PPO formed new H-bonds with residues K90 and T193, resulting in easier substrate binding (low K_M) and activity (high k_{cat}). Additionally, the two newly formed H-bonds (T193···PPO and K90···PPO) in GluDH3_V375G were present over a shorter timespan (≈ 5.5 ns) than that of GluDH3_V375S (**Fig. S9**). It may explain that the GluDH3_V375G displayed lower activity than that of GluDH3_V375S. Furthermore, to investigate the synergistic effect of the residues at positions 90 and 753, a combinatorial library (K90-V375) was constructed and screened (GluDH3_V375S as the reference). However, nearly all the variants showed dramatically decreased activity. The variants showing high activity had the same sequence as GluDH3_V375S, which indicated that K90-S375 is the best pair in GluDH3 for the desired activity.

3.5 Prediction of key features in the desired AADHs for L-PPT synthesis

Based on the above enzyme-ligand docking and MD simulations analysis, a new H-bond network was built in the GluDH3 GluDH3_V375S model, in which the beneficial substitution V375S decreased the steric hindrance with the assistance of polar residues at positions 90 and 193. Substrate PPO was located in an active site-decorating α-helix that contains the residues from 371 to 385. Position 375 plays an important role in the substrate recognition of the phosphoryl group of PPO, while two polar or charged residues (T193 and K90) that are conserved in the GluDH family are responsible for PPO stabilization. Furthermore, when the V375S substitution was introduced into the ten enzymes, improved activity was only observed in the GluDHs harboring these two crucial residues (K_{90} and T_{193}) (**Table 3**). Aside from variant E_3+V375S, the other three variants of E_4+V375S, E_5+V375S and E_6+V375S showed 67.4, 178 and 282-fold increases in specific activity compared to the WTs, respectively. However, after the introduction of V375S into E1, E2, E7, E8, E9 and E10, no improvement was observed. Notably, only the serine replacement was the best choice for activity improvement among the 19 residues in the analysis of all the E3 variants (**Fig. 4**), which explained our assumption that the introduction of a polar interaction at position 375 with the assistance of two polar and charged residues constituted a stronger H-bond network, which

dramatically enhanced the binding of PPO. We hypothesized that these two residues were crucial to the desired asymmetric amination activity.

Using this information, a strategy was developed to identify the "glufosinate dehydrogenase" with the desired reductive amination activity towards PPO (**Fig. 5**). First, potential GluDH-coding sequences were searched using GluDH3 as a template (>50% sequence similarity, **Table S2**). Based on the above-mentioned results, K90 and T193 were the two crucial residues for the desired amination activity. Thus, a sequence analysis was performed to exclude enzymes that did not contain the featured sequence (K90 and T193). Then, the selected GluDH-coding genes were synthesized and expressed in *E. coli*. The GluDH variants were constructed by introducing V375S, and the activity of the GluDH WT and variants were investigated. By using this strategy, forty GluDH genes from the NCBI database were selected and expressed in the same vector and host. As expected, all the variants containing beneficial substitution V375S exhibited significant improvements in reductive amination activity towards PPO compared with the corresponding WTs. Improvements between the WT and WT+V375S ranged from 2.1 to 272 folds (**Table S3**). For convenience, these GluDH variants with improved activity were named "glufosinate dehydrogenases" (GfDHs). These results suggested that GluDHs with the featured sequences can be engineered into GfDHs. These findings confirmed that GfDHs can be achieved by only introducing one substitution into GluDHs harboring the featured sequences, which also provide an applicable toolbox of GfDHs for the industrialization of L-phosphinothricin.

3.6 Asymmetric reductive amination of PPO employing whole cells of recombinant *E. coli* harboring GfDH and GDH

To evaluate the practical catalytic effect of variant GluDH3_V375S, the asymmetric amination efficiency of variant GluDH3_V375S and its WT (GluDH3) were tested toward higher substrate loading under optimized conditions (pH 6.5 and 35 °C). To regenerate the cofactor NADPH, a D-glucose dehydrogenase from *Exiguobacterium sibiricum* (*Es*GDH) was co-expressed in *E. coli*. In the reaction mixture, 100 mM PPO (17.8 $g \cdot L^{-1}$) with 120 mM glucose as co-substrate, 150 mM $(NH_4)_2SO_4$ as an amino donor, and 0.5 mM of extra cofactors were mixed. The substrate was completely converted to L-PPT (conversion >99%, >99% *e.e.*) within 30 min using 5 $g \cdot L^{-1}$

lyophilized *E. coli* co-expressing GluDH3_V375S and *Es*GDH. The conversion can only reach 93% after 24 h of employing GluDH3_WT due to its low activity (**Fig. 6**). These results clearly demonstrated the great potential of variant GluDH3_V375S in the large-scale production of L-PPT. To explore the performance of GluDH3_V375S, the substrate concentration was gradually increased from 100 mM to 300 mM and 500 mM, and the ammonium and glucose concentrations were also increased to the same extent. As shown in **Fig. 6**, the conversion of 0.5 M PPO (89.04 $g \cdot L^{-1}$) can still reach nearly 100% after 0.5-1 h reaction with the same amount of biocatalyst (5 $g \cdot L^{-1}$ dry cells harboring GluDH3_V375S and *Es*GDH), affording an L-PPT product with *e.e.* > 99%. The space-time yield of the process reached up to 4752 $g \cdot L^{-1} \cdot d^{-1}$, which markedly exceeds the average productivity of industrial bioprocesses (372 $g \cdot L^{-1} \cdot d^{-1}$), and it is 258-fold higher than the GluDH3_WT-catalyzed reaction (18.4 $g \cdot L^{-1} \cdot d^{-1}$). Furthermore, in comparison with the reported amidase and transaminase-involved reaction (**Table S4**), GluDH3_V375S displayed the highest conversion and the shortest reaction time when the substrate loading reached 89.04 g/L. Moreover, the cost of producing a crude product containing 1 ton of L-PPT was roughly calculated (**Table S5**). When considering the substrate, biocatalyst and co-enzyme, approximately €22776 is needed to produce 1 ton of L-PPT by using GfDH and the GDH-catalyzed reaction, which is a bit higher than the cost of transaminase-involving production (€20170/ ton). However, for the latter, an additional and difficult process is required to separate the L-PPT and PPO due to the low conversion of the transaminase-catalyzed reaction and the similar physical and chemical properties of PPO and PPT. Taken together, these data show that GluDH3_V375S mediated a biocatalytic cascade system to give excellent enantioselectivity and the highest enzyme activity and productivity, making it promising and competitive for the synthesis of L-PPT at an industrial scale.

4 Conclusions

In summary, a glutamate dehydrogenase named GluDH3 from *Pseudomonas monteilii* was selected for engineering with the desired asymmetric reductive amination activity towards PPO. After screening, the variant GluDH3_V375S exhibited a dramatic improvement in its reductive amination activity towards PPO. The proposed mechanism was that the serine substitution increased the polar interaction between K90, T193, and the substrate PPO. During the asymmetric reductive

amination of PPO to L-PPT, to the best of our knowledge, the variant GluDH3_V375S-catalysed bioprocess exhibited the highest production and space-time yield (up to 4.752 $kg \cdot L^{-1} \cdot d^{-1}$), indicating that it is a promising biocatalyst for practical applications in the production of L-PPT. Furthermore, based on the docking analysis, MD simulation and experimental data, tuning glutamate dehydrogenases to have featured sequences can generate more suitable "glufosinate dehydrogenases" for producing chiral L-phosphinothricin.

Funding

This work was funded by the National Natural Science Foundation of China (No. 31970046, No. 21978268 and No. 31700693) and the Fundamental Research Funds for the Provincial Universities of Zhejiang (RF-A2019010).

Declaration of conflict of interest

There are no conflicts to declare.

CRediT author statement

Feng Cheng: Conceptualization, Investigation, Writing-Original draft preparation; **Heng Li:** Data curation, Writing-Original draft preparation, Methodology; **Kai Zhang:** Visualization, Investigation; **Qing-Hua Li:** Data curation, Investigation; **Dong Xie:** Visualization; **Ya-Ping Xue:** Writing-Reviewing and Editing, Project administration; **Yu-Guo Zheng:** Supervision.

Declaration of interests

The authors declare that they have no known competing financial interests or personal relationships that could have appeared to influence the work reported in this paper.

References

Albizati, K.F., Kambourakis, S., Grubbs, A., Borer, B.C., 2017 Process of producing phosphinothricin employing nitrilases. U.S. Patents. 8981142 https://patents.google.com/patent/US8981142B2/en

Baker, P.J., Britton, K.L., Engel, P.C., Farrants, G.W., Lilley, K.S., Rice, D.W., Stillman, T.J., 1992 Subunit assembly and active site location in the structure of glutamate dehydrogenase. Proteins: Struct., Funct., Bioinf. 12, 75-86. https://doi.org/10.1002/prot.340120109

Baker, P.J., Waugh, M.L., Wang, X.G., Stillman, T.J., Turnbull, A.P., Engel, P.C., Rice, D.W., 1997 Determinants of substrate specificity in the superfamily of amino acid dehydrogenases. Biochemistry 36, 16109-16115. https://doi.org/10.1021/bi972024x

Bartsch, K., Kriete, G., Broer, I., 2001 Genes coding for amino acid deacetylases with specificity for N-acetyl-L-phosphinothricin, their isolation and their use. U.S. Patents. 6177616 https://patents.google.com/patent/US6177616B1/en

Bommarius, A.S., Au, S.K., 2015 Science of Synthesis: Biocatalysis in Organic Synthesis, in: Faber,K., Fessner, W.D., Turner, N.J. (Eds), Thieme Verlag., Stuttgart, pp. 335-358.

Brunhuber, N.M.W., Blanchard, J.S., 1994 The Biochemistry and Enzymology of Amino Acid Dehydrogenases. Crit. Rev. Biochem. Mol. Biol. 29, 415-467. https://doi.org/10.3109/10409239409083486

Brunharo, C.A.C.G., Takano, H.K., Mallory-Smith, C.A., Dayan, F.E., Hanson, B.D., 2019 Role of Glutamine Synthetase Isogenes and Herbicide Metabolism in the Mechanism of Resistance to Glufosinate in *Lolium perenne* L. spp. *multiflorum* Biotypes from Oregon. J Agr Food Chem. 67, 8431-8440. https://doi.org/10.1021/acs.jafc.9b01392

Busca, P., Paradisi, F., Moynihan, E., Maguire, A.R., Engel, P.C., 2004 Enantioselective synthesis of non-natural amino acids using phenylalanine dehydrogenases modified by site-directed mutagenesis. Org. Biomol. Chem. 2, 2684-2691. https://doi.org/10.1039/B406364C

Cheng, F, Chen X.L., Xiang C., Liu Z.Q., Wang Y.J., Zheng Y.G. 2020 Fluorescence-based high-throughput screening system for R-ω-transaminase engineering and its substrate scope extension. Appl Microbiol Biotechnol, https://doi.org/10.1007/s00253-020-10444-y

Cheng, F., Tang, X.L., Kardashliev, T., 2018 Transcription factor-based biosensors in high-throughput screening: advances and applications. Biotechnol J. 13, 1700648. https://doi.org/10.1002/biot.201700648

Cheng, F., Zhu, L., Schwaneberg, U., 2015 Directed evolution 2.0: improving and deciphering enzyme properties. Chem. Commun. 51, 9760-9772. https://doi.org/10.1039/C5CC01594D

Geng, F., Ma, C.W., Zeng, A.P., 2017 Reengineering substrate specificity of *E. coli* glutamate dehydrogenase using a position-based prediction method. Biotechnol. Lett. 39, 599-605. https://doi.org/10.1007/s10529-017-2297-2

Hoerlein, G., 1994 Glufosinate (Phosphinothricin), A Natural Amino Acid with Unexpected

Herbicidal Properties. In: Ware, G.W. (Ed.), Springer New York, New York, pp. 73-145.

Hummel, W., Gröger, H., 2012 Enzyme Catalysis in Organic Synthesis, in: Drauz, K., Gröger, H., May, O. (Eds), Wiley-VCH., Weinheim, 2012, pp. 1165-1203

Jia, D.X., Liu, Z.J., Xu, H.P., Li, J.L., Li, J.J., Jin, L.Q., Cheng, F., Liu, Z.Q., Xue, Y.P., Zheng, Y.G., 2019 Asymmetric synthesis of L-phosphinothricin using thermostable alpha-transaminase mined from *Citrobacter koseri*. J. Biotechnol. 302, 10-17. https://doi.org/10.1016/j.jbiotec.2019.06.008

Jin, L.Q., Peng, F., Liu, H.L., Cheng, F., Jia, D.X., Xu, J.M., Liu, Z.Q., Xue, Y.P., Zheng, Y.G., 2019 Asymmetric biosynthesis of L-phosphinothricin by a novel transaminase from *Pseudomonas fluorescens* ZJB09-108. Process Biochem. 85, 60-67. https://doi.org/10.1016/j.procbio.2019.07.010

Kang, X.M., Cai, X., Liu, Z.Q., Zheng, Y.G., 2019a Identification and characterization of an amidase from Leclercia adecarboxylata for efficient biosynthesis of L-phosphinothricin. Bioresour. Technol. 289, 121658. https://doi.org/10.1016/j.biortech.2019.121658

Kang, X.M., Zhang, X.J., Hong, L.L., Peng, F., Liu, Z.Q., Zheng, Y.G., 2019b Establishment of a novel high-throughput screening method for the detection and quantification of L-phosphinothricin produced by a biosynthesis approach. Process Biochem. 76, 136-141. https://doi.org/10.1016/j.procbio.2018.10.015

Khorsand, F., Murphy, C.D., Whitehead, A.J., Engel, P.C., 2017 Biocatalytic stereoinversion of D-para-bromophenylalanine in a one-pot three-enzyme reaction. Green Chem. 19, 503-510. https://doi.org/10.1039/C6GC01922F

Li, H., Liao, J.C., 2014 Development of an NADPH-dependent homophenylalanine dehydrogenase by protein engineering. ACS Synth. Biol. 3, 13-20. https://doi.org/10.1021/sb400093x

Paradisi F, Collins S, Maguire A.R., Engel P.C., 2007 Phenylalanine dehydrogenase mutants: efficient biocatalysts for synthesis of non-natural phenylalanine derivatives. J Biotechnol. 128, 408-411. https://doi.org/doi:10.1016/j.jbiotec.2006.08.008

Prakash, P., Punekar, N.S., Bhaumik, P., 2018 Structural basis for the catalytic mechanism and alpha-ketoglutarate cooperativity of glutamate dehydrogenase. J. Biol. Chem. 293, 6241-6258. https://doi.org/10.1074/jbc.RA117.000149

Ricca, E., Brucher, B., Schrittwieser, J.H., 2011 Multi-enzymatic cascade reactions: overview and

perspectives. Adv Synth Catal. 353, 2239-2262. https://doi.org/10.1002/adsc.201100256

Rojas-Cervellera, V., Ardèvol, A., Boero, M., Planas, A., Rovira, C., 2013 Formation of a covalent glycosyl-enzyme species in a retaining glycosyltransferase. Chem. - Eur. J. 19, 14018-14023. https://doi.org/10.1002/chem.201302898

Seah, S.Y.K., Linda Britton, K., Baker, P.J., Rice, D.W., Asano, Y., Engel, P.C., 1995 Alteration in relative activities of phenylalanine dehydrogenase towards different substrates by site-directed mutagenesis. FEBS Lett. 370, 93-96. https://doi.org/10.1016/0014-5793(95)00804-I

Sharma, M., Mangas-Sanchez, J., Turner, N.J., Grogan, G., 2017 NAD(P)H-Dependent Dehydrogenases for the Asymmetric Reductive Amination of Ketones: Structure, Mechanism, Evolution and Application. Adv Synth Catal. 359, 2011-2025. https://doi.org/10.1002/adsc.201700356

Sharma, M., Mangas-Sanchez, J., France, S.P., Aleku, G.A., Montgomery, S.L., Ramsden, J.I., Turner, N.J., Grogan, G., 2018 A Mechanism for Reductive Amination Catalyzed by Fungal Reductive Aminases. Acs Catal. 8, 11534-11541. https://doi.org/10.1021/acscatal.8b03491

Singh, M., Singh, S., Deshaboina, S., Krishnen, H., Lloyd, R., Holt-Tiffin, K., Bhattacharya, A., Bandichhor, R., 2012 Asymmetric reduction of a key intermediate of eslicarbazepine acetate using whole cell biotransformation in a biphasic medium. Catal. Sci. Technol. 2, 1602-1605. https://doi.org/10.1039/C2CY00537A

Son, H.F., Kim, I.K., Kim, K.J., 2015 Structural insights into domain movement and cofactor specificity of glutamate dehydrogenase from Corynebacterium glutamicum. Biochem. Biophys. Res. Commun. 459, 387-392. https://doi.org/10.1016/j.bbrc.2015.02.109

Srivastava, G., Pal, M., Kaur, S., Jolly, R.S., 2015 A highly efficient designer cell for enantioselective reduction of ketones. Catal. Sci. Technol. 5, 105-108. https://doi.org/10.1039/C4CY01017E

Tan, S., Evans, R., Singh, B., 2006 Herbicidal inhibitors of amino acid biosynthesis and herbicide-tolerant crops. Amino Acids 30, 195-204. https://doi.org/10.1007/s00726-005-0254-1

Tomita, T., Yin, L., Nakamura, S., Kosono, S., Kuzuyama, T., Nishiyama, M., 2017 Crystal structure of the 2-iminoglutarate-bound complex of glutamate dehydrogenase from Corynebacterium glutamicum. Febs Lett. 591, 1611-1622. https://doi.org/10.1002/1873-3468.12667

Uppada, V., Bhaduri, S., Noronha, S.B., 2014 Cofactor regeneration–an important aspect of biocatalysis. Curr. Sci. 946-957. https://www.jstor.org/stable/24102378

Xu, J.M., Cheng, F., Fu, F.T., Hu, H.F., Zheng, Y.G., 2017 Semi-Rational Engineering of Leucine Dehydrogenase for L-2-Aminobutyric Acid Production. Appl Biochem Biotech. 182, 898-909. https://doi.org/10.1007/s12010-016-2369-0

Xue, Y.P., Cao, C.H., Zheng, Y.G., 2018 Enzymatic asymmetric synthesis of chiral amino acids. Chem. Soc. Rev. 47, 1516-1561. https://doi.org/10.1039/C7CS00253J

Yin, X., Wu, J., Yang, L., 2018 Efficient reductive amination process for enantioselective synthesis of L-phosphinothricin applying engineered glutamate dehydrogenase. Appl Microbiol Biotechnol. 102, 4425-4433 https://doi.org/10.1007/s00253-018-8910-z

Zhu, D., Hua, L., 2009 Biocatalytic asymmetric amination of carbonyl functional groups – a synthetic biology approach to organic chemistry. Biotechnol. J. 4, 1420-1431. https://doi.org/10.1002/biot.200900110

Zhu, L., Wu, Z., Jin, J.-M., Tang, S.-Y., 2016 Directed evolution of leucine dehydrogenase for improved efficiency of L-tert-leucine synthesis. Appl Microbiol Biotechnol. 100, 5805-5813. https://doi.org/10.1007/s00253-016-7371-5

Scheme 1. Asymmetric amination of PPO to L-PPT by whole cells of recombinant *E. coli* harboring GluDH and GDH.

Fig 1. Evolutionary tree of AADH protein sequences. The selected E1-E10 were located in the different groups of glutamate dehydrogenase (GluDH), leucine dehydrogenase (LeuDH), and phenylalanine dehydrogenase (PheDH).

Fig 2. Identification of beneficial GluDH variants from five small focused gene libraries. (a) Thirty-eight beneficial variants were selected after preliminary screening and their relative activities. The relative activity is shown according to the fluorescence intensity. (b) The specific activity of the WT and its variants WT+V375S and WT+V375G. The activity was measured using a standard enzyme activity assay.

Fig 3. Insights on PPO (in stick form) in the substrate-binding pockets of the wild-type (a and c) and variant GluDH3_V375S (b and d). The substrate-binding pockets are displayed in surface form. The hydrogen bonds between the residues and PPO are shown as red dashes. Carbon, nitrogen and oxygen atoms are shown in cyan, blue and red, respectively. Protons are shown in grey in (a) and (b), while the protons are hidden in (c) and (d).

Fig 4. Comparison of the activity of GluDH3 variants (mutation at position 375). The X-axis represents different amino acid substitutions, while the Y-axis represents the improvement in activity compared to GluDH3_WT (determined by HPLC). The assay conditions contain the following: 20 mM PPO, 0.1 M phosphate buffer (pH=7.2), 25 mM glucose, 50 mM ammonium sulfate, 1 mM $NADP^+$, 25 g/L GluDH3 variants and GDH at 35°C.

Fig 5. The established flow chart of the *in silico* and experiment combined approach for the identification of "glufosinate dehydrogenase" with the desired reductive amination activity towards PPO (steps A–H). The protein engineering strategies for AADH to GluDH are represented in the first module (green colored boxes). The process from GluDH to GfDH is shown in the second module (blue colored boxes).

Fig 6. Batch production of L-PPT from PPO with GluDH3 wild-type and variant GluDH3_V375S by coupling with EsGDH for NADPH regeneration. The substrate concentrations were set at 100, 300 and 500 mM. The reactions were performed in 0.1 M phosphate buffer (pH 6.5) at 35 °C.

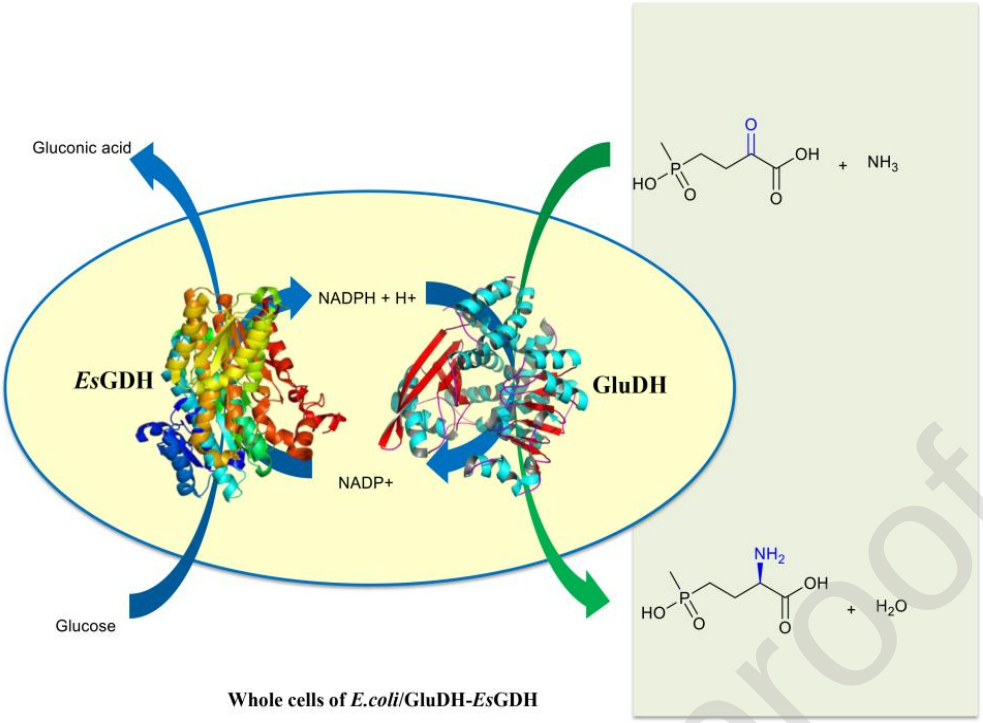

Scheme 1.

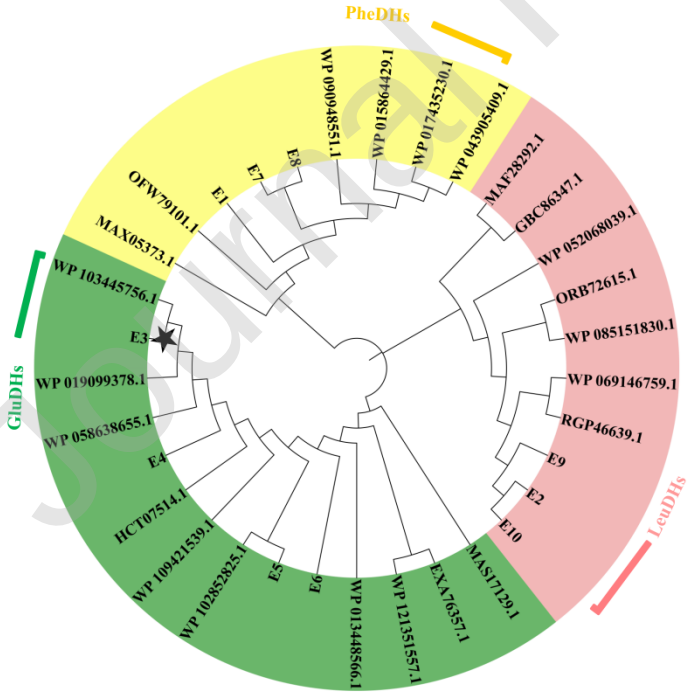

Fig 1.

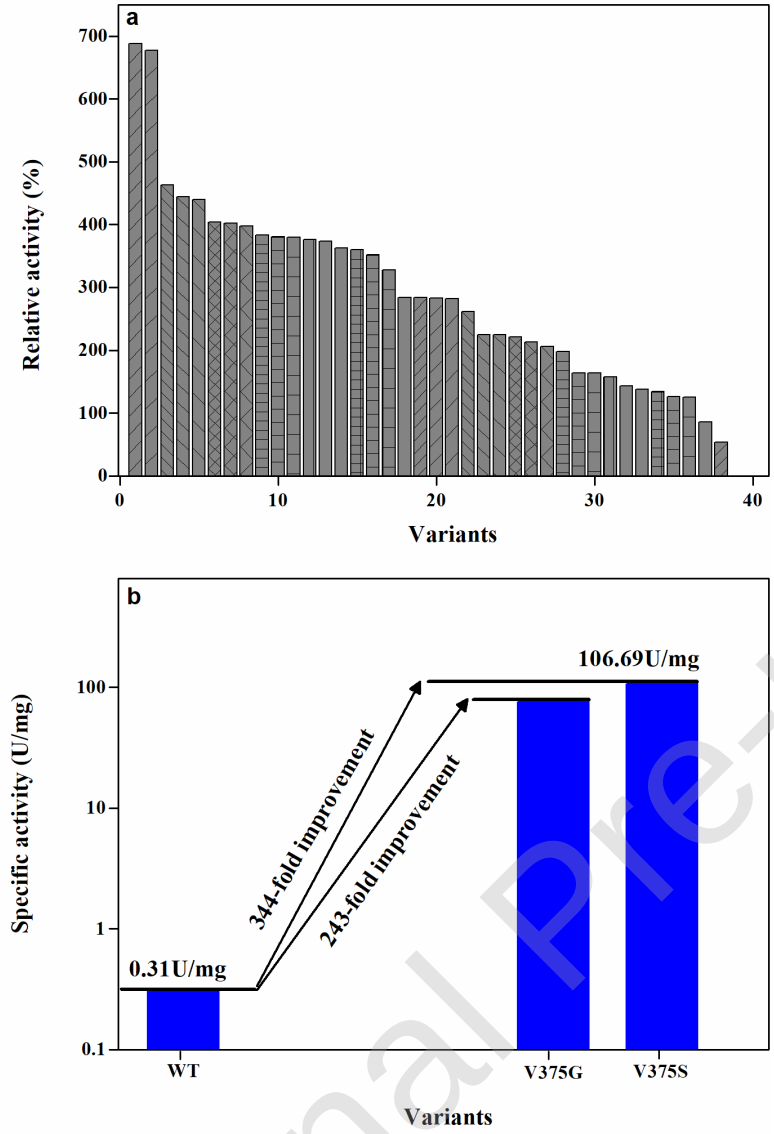

Fig 2.

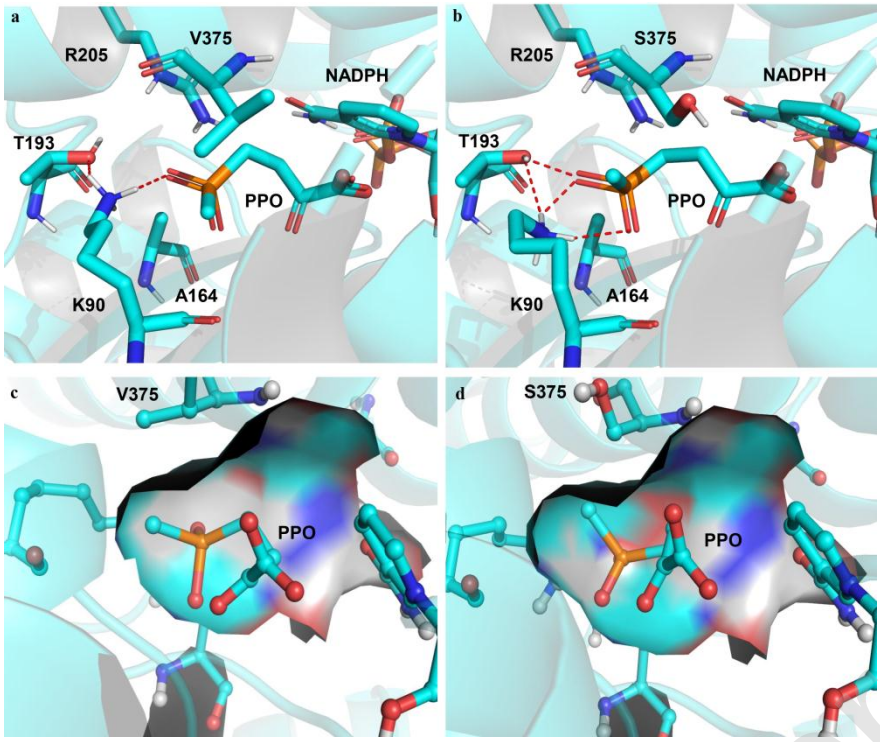

Fig 3.

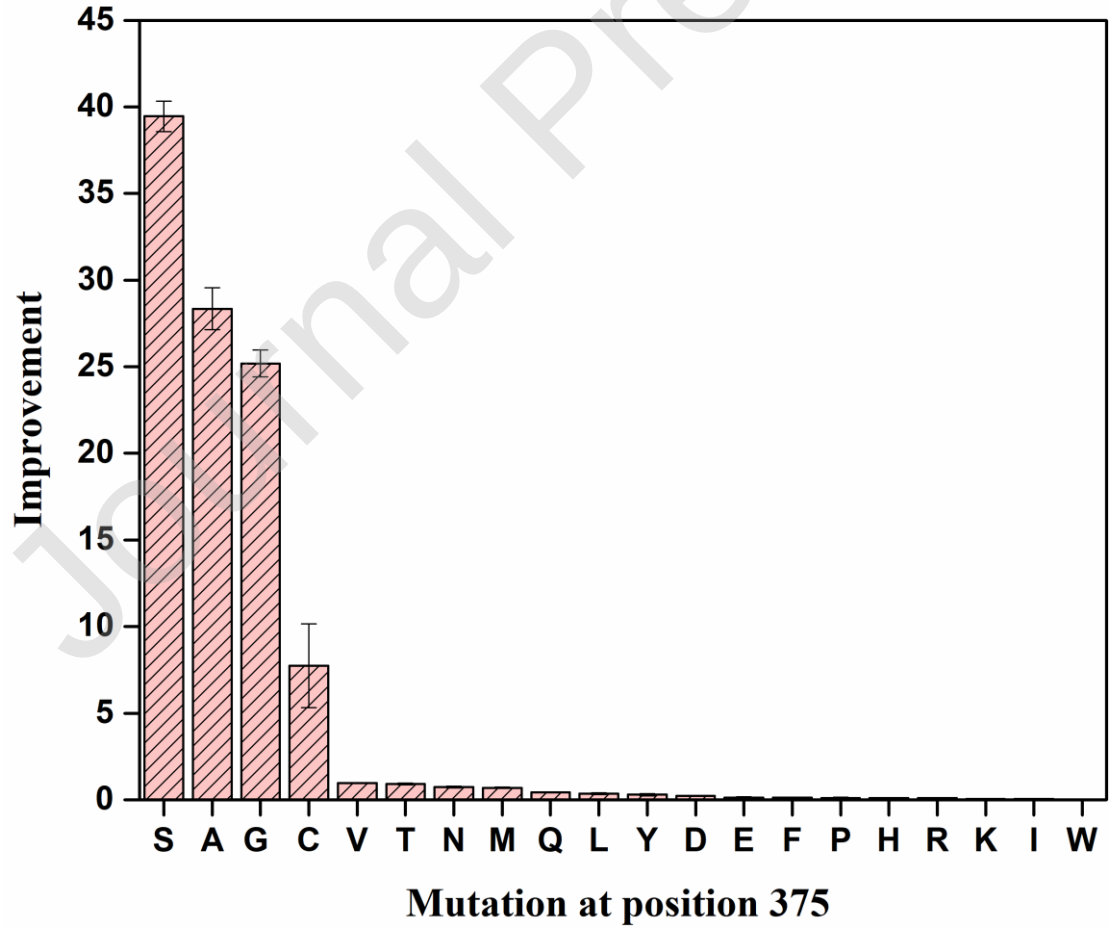

Fig 4.

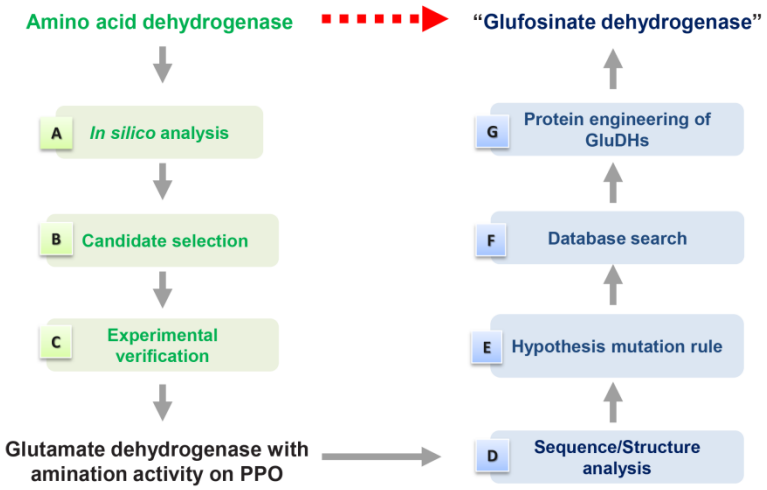

Fig 5.

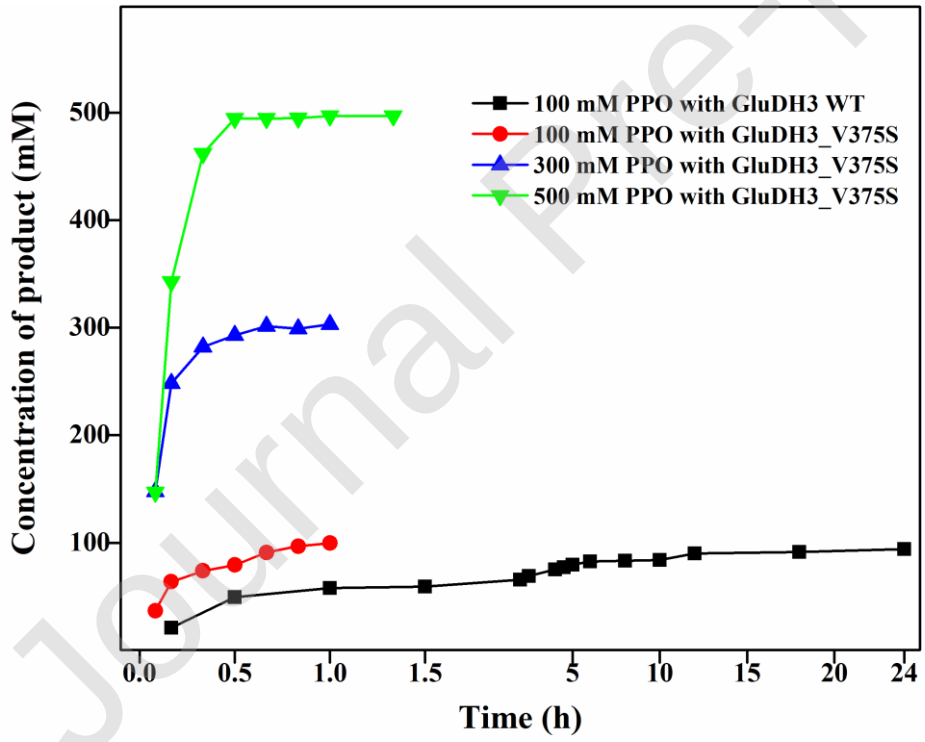

Fig 6. Batch production of L-PPT from PPO with GluDH3 wild-type and variant GluDH3_V375S by coupling with EsGDH for NADPH regeneration. Substrate concentrations were set at 100, 300 and 500 mM. Reactions were performed in 0.1 M phosphate buffer (pH 6.5) and at 35 °C.

Table 1. The activity and enantioselectivity of selected AADHs towards PPO.

Serial number	Category	Genbank number	Origin	Specific activity (U/g)	e.e. (%)	Recombinant protein yield (g/L)[a]
1LEH	NADH-Specific LeuDH	1LEH[b]	*Lysinibacillus sphaericus*	0.71±0.03	>86	0.45±0.06
1BW9	NADH-Specific PheDH	1BW9[b]	*Rhodococcus* sp.	1.98±0.32	>81	0.41±0.04
5IJZ	NADPH-Specific GluDH	5IJZ[b]	*Corynebacterium glutamicum* ATCC 14067	19.58±2.88	>90	0.38±0.06
E_1	NADH-Specific LeuDH	WP_048392303	*Lysinibacillus*	6.03±0.25	>78	0.53±0.08
E_2	NADH-Specific PheDH	WP_115963497	*Rhodococcus* sp. OK269	0.93±0.27	>72	0.60±0.05
E_3	NADPH-Specific GluDH	WP_060477601.1	*Pseudomonas monteilii*	328.77±3.33	>99	0.44±0.01
E_4	NADPH-Specific GluDH	WP_042124798.1	*Pseudomonas japonica*	193.63±1.79	>99	0.32±0.02
E_5	NADPH-Specific GluDH	WP_023446861.1	*Pseudomonas stutzeri*	172.72±5.18	>99	0.43±0.01
E_6	NADPH-Specific GluDH	WP_101496154.1	*Thiopseudomonas denitrificans*	121.10±3.41	>99	0.39±0.01
E_7	NADH-Specific LeuDH	WP_113734247.1	*Bacillus* sp. SRB_331	5.30±2.52	>92	0.34±0.03
E_8	NADH-Specific LeuDH	WP_000171355.1	*Bacillus* sp.	7.14±2.07	>90	0.14±0.01
E_9	NADH-Specific PheDH	WP_008712434.1	*Rhodococcus* sp. AW25M09	0.92±0.81	>81	0.25±0.02
E_{10}	NADH-Specific PheDH	WP_115963497.1	*Rhodococcus* sp. OK269	0.51±0.12	>85	0.45±0.02

[a]: The recombinant protein yield refers to the soluble recombinant AADH concentration (as measured by BCA protein assay protocol) per volume of fermentation with standard culture and induction conditions using BL21(DE3) as the blank control. [b]: the number refers to the PDB ID.

Table 2. Kinetic parameters of GluDH3_WT and variant GluDH3_V375S

Enzyme	V_{max} ($U \cdot mg^{-1}$)	K_m^A (mM)	K_m^B (mM)	k_{cat} (s^{-1})	Ks^A ($s^{-1} \cdot mg^{-1}$)	K_m^B (mM)	k_{cat}/K_m^B ($mM^{-1} \cdot s^{-1}$)
WT	40.65	0.17	19.21	33.24±1.49	0.028	19.21	1.73

V375S	1578.17	0.12	4.43	1290.42±17.85	0.032	4.43	291.02

Note: The kinetic parameters were calculated using the equation $v = \frac{v_{max[A][B]}}{[A][B]+[B]K_m^A+[A]K_{m+}^B K_m^B K_s^A}$. [A] and [B] are the NADPH and PPO concentrations, respectively. V_{max} is the maximum reaction rate, and K_M^A and K_M^B are the apparent substrate affinities toward NADPH and PPO, respectively. Ks^A represents the dissociation constant between GfDH and NADPH. Kinetic characterizations were performed in 0.1 M phosphate buffer (pH 6.5) at 35°C with 0.5-20 mM PPO, 50 mM $(NH4)_2SO_4$, 1-10 mM NADPH and purified enzymes.

Table 3. Key motifs based on a section of a multiple sequence alignment for selected enzymes

Entry	Residue at position 90	Residue at position 193	Improved fold between WT and WT+V375S[a]
E1	39 ALGGA	131 NYVTG	0.91±0.18
E2	38 AAGGT	135 KFVFG	0.70±0.11
E3	89 YKGGL	190 SVLTG	344±8.25
E4	89 YKGGL	190 SVLTG	67.4±7.00
E5	89 YKGGL	190 SVLTG	178±3.0
E6	89 YKGGI	190 SVFTG	282±26.47
E7	41 ALGGT	133 DFVTG	0.87±0.14
E8	41 ALGGT	133 DFVTG	0.72±0.05
E9	38 AAGGT	135 EFVFG	0.74±0.09
E10	38 AAGGT	135 KFVFG	0.67±0.12

[a]: Reaction conditions: 20 mM PPO, 0.1 M phosphate buffer (pH=7.2), 25 mM glucose, 50 mM ammonium sulfate, 1 mM $NADP^+$, 25 g/L AADHs and GDH crude enzyme, 35 °C, 600 rpm per volume of fermentation.

Table 4 The specific activity of GluDH3_WT and GluDH3_V375S towards α-keto acids

Substrate	Substrate structure	Specific activity(U/g)[a] GluDH3_WT	GluDH3_V375S
PPO	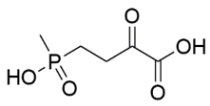	526.3±1.27	(95.40±6.45) ×10^3

pyruvic acid	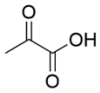	6.71±0.77	0.53±0.11
2-oxobutyric acid	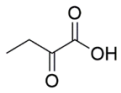	222.7±3.25	18.79±1.96
3-methyl-2-oxobutanoic acid	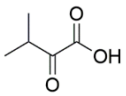	12.89±1.46	1.76±0.45
2-oxopentanoic acid	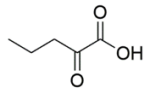	277.5±3.58	131.5±1.22
α-ketoglutarate	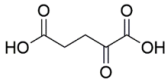	9131±2.80	(45.7±1.25)×10^3
2-oxo-2-phenylacetic acid	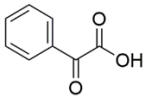	1.09±0.21	N.D.[b]
2-oxo-3-phenylpropanoic acid	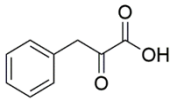	N.D.[b]	N.D.[b]
3-hydroxy-2-oxo-3-phenylpropanoic acid	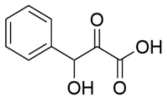	3.82±1.36	4.31±0.95

a: The specific activity was determined by measuring the decrease in NADPH at 340 nm. The reaction was performed at 35°C, 600 rpm for 30 min (reaction conditions: 1 mL final volume consisting of 20 mM substrates, 0.1 M phosphate buffer (pH=7.2), 50 mM ammonium sulfate, 10 mM NADPH, and purified enzymes).

N.D: not detectable.